Univariate and Multivariate Generalized Multiscale Entropy to Characterise EEG Signals in Alzheimer's Disease

entropy

MDPI

Article

Univariate and Multivariate Generalized Multiscale Entropy to Characterise EEG Signals in Alzheimer's Disease

Hamed Azami [1,*], Daniel Abásolo [2], Samantha Simons [2] and Javier Escudero [1]

[1] Institute for Digital Communications, School of Engineering, University of Edinburgh, Edinburgh EH9 3FB, UK; javier.escudero@ed.ac.uk

[2] Centre for Biomedical Engineering, Department of Mechanical Engineering Sciences, Faculty of Engineering and Physical Sciences, University of Surrey, Guildford GU2 7XH, UK; d.abasolo@surrey.ac.uk (D.A.); s.simons@surrey.ac.uk (S.S.)

* Correspondence: hamed.azami@ed.ac.uk; Tel.: +44-748-147-8684

Academic Editor: Anne Humeau-Heurtier
Received: 29 October 2016; Accepted: 9 January 2017; Published: 12 January 2017

Abstract: Alzheimer's disease (AD) is a degenerative brain disorder leading to memory loss and changes in other cognitive abilities. The complexity of electroencephalogram (EEG) signals may help to characterise AD. To this end, we propose an extension of multiscale entropy based on variance (MSE_{σ^2}) to multichannel signals, termed multivariate MSE_{σ^2} ($mvMSE_{\sigma^2}$), to take into account both the spatial and time domains of time series. Then, we investigate the $mvMSE_{\sigma^2}$ of EEGs at different frequency bands, including the broadband signals filtered between 1 and 40 Hz, θ, α, and β bands, and compare it with the previously-proposed multiscale entropy based on mean (MSE_{μ}), multivariate MSE_{μ} ($mvMSE_{\mu}$), and MSE_{σ^2}, to distinguish different kinds of dynamical properties of the spread and the mean in the signals. Results from 11 AD patients and 11 age-matched controls suggest that the presence of broadband activity of EEGs is required for a proper evaluation of complexity. MSE_{σ^2} and $mvMSE_{\sigma^2}$ results, showing a loss of complexity in AD signals, led to smaller p-values in comparison with MSE_{μ} and $mvMSE_{\mu}$ ones, suggesting that the variance-based MSE and mvMSE can characterise changes in EEGs as a result of AD in a more detailed way. The p-values for the slope values of the mvMSE curves were smaller than for MSE at large scale factors, also showing the possible usefulness of multivariate techniques.

Keywords: Alzheimer's disease; complexity; multivariate generalized multiscale entropy; statistical moments; electroencephalogram

1. Introduction

Alzheimer's disease (AD) is a progressive neurodegenerative disease and the most common form of dementia in the elderly population, affecting intellectual, behavioural, and functional abilities [1–3]. A positive diagnosis of AD allows the patient and his/her family time to be informed about the disease, to make life and financial decisions, and to plan for the future. In contrast, a negative diagnosis may reduce worry about memory loss associated with ageing. Moreover, it permits for early treatments of reversible conditions with similar symptoms (like depression and nutrition or medication problems) [2]. Medical-based diagnosis of AD is not fully reliable and symptoms are frequently dismissed as normal consequences of healthy ageing. Spinal fluid analysis and signal and image processing methods are used to increase the confidence of the diagnosis of AD [2,3].

As AD progresses, there are changes in the dynamical brain activity that can be recorded in electroencephalogram (EEG) signals [1,2]. The EEG is an affordable, portable, and non-invasive tool to assess brain activity [4]. In addition, in comparison with other non-invasive brain imaging approaches,

EEG has high temporal resolution and includes essential information about abnormal brain dynamics in AD subjects [2]. The studies show that AD causes a spectral slowdown and alterations in the non-linear dynamics of the brain signal [5,6].

A prevailing approach to diagnose of AD is to consider specific frequency bands in EEG, such as δ (1–4 Hz), θ (4–8 Hz), α (8–13 Hz), β (13–30 Hz), and γ (30–40 Hz) [2,7,8]. AD affects these different frequency bands in different ways. An increase of power in δ, θ, and γ, and a decrease of power in higher frequencies α and β have been reported in AD patients in comparison with healthy age-matched control subjects [2,7–9].

In recent years, because of the non-linearity in the brain, even at the neuronal level [10], there has been an increasing interest in non-linear techniques for the analysis of EEGs for diagnosis of AD [1,2,11–13]. One of the most popular non-linear concepts used to assess the dynamical characteristics of signals is that of entropy [14,15]. This concept measures the uncertainty and irregularity of a time series [14,15]. Higher entropy normally stands for higher uncertainty, whereas lower entropy shows more regularity and certainty in a signal [14,16]. Thus, it can be considered as an indicator of dynamical changes along the temporal evolution of EEG signals.

Entropy approaches have been broadly used to characterise different kinds of signals. However, they achieve their maxima for signals with no structure (random) and are defined only for a single temporal scale: the one associated with the original sampling of the time series [17,18]. This can be considered as a limitation to investigate dynamics at longer time scales. Accordingly, multiscale entropy (MSE) was proposed to define entropy values for a range of scales to evaluate the complexity of signals at different time scales [17]. Thus, MSE quantifies signal complexity, which may remain hidden for basic entropy approaches [19].

Complexity indicates a degree of structural richness [19]. In fact, neither completely regular (periodic) nor completely irregular (uncorrelated random) time series are truly complex, because none of them is structurally rich at a global level. Thus, the concept of irregularity and complexity are not the same. For example, white Gaussian noise (WGN) is more irregular than $1/f$ noise, although the latter is more complex. It is in agreement with this fact that the WGN does not have a rich structure and shows a rapid drop in entropy with an increase in time scale factor [19–21].

The MSE algorithm at the temporal scale factor λ includes two main steps [17]. First, in the coarse-graining process, the original signal is divided into non-overlapping segments with length λ, and then the average of each segment is calculated. Second, the sample entropy (SampEn) [15] of the coarse-grained time series is computed [17].

For multi-channel signals, the MSE algorithms, though powerful and broadly-used, treat individual time series separately. Therefore, this method is appropriate for the components of multi-channel time series that are statistically independent. However, real multivariate physiological signals are simultaneously recorded and the time series are statistically dependent [22,23]. To this end, multivariate MSE using the mean in the coarse-graining process, named mvMSE_{μ}, has been recently introduced [22]. The mvMSE_{μ} algorithm was validated on both illustrative benchmark signals and on real-world multivariate physiological and non-physiological datasets [22,24].

However, the dynamics of the volatility (variance) of a time series over multiple temporal scales to extract dynamical properties of spread also need to be inspected. To this end, Costa and Goldberger have recently proposed a modified MSE where the variance is used in the coarse-graining process [25]. The mean- and variance-based MSE would be referred to as MSE_{μ} and MSE_{σ^2}, respectively. MSE_{σ^2} was used to analyse heartbeat signals from healthy young and older subjects and patients with congestive heart failure syndrome. It was demonstrated that the dynamics of the volatility of heartbeat signals obtained from healthy young subjects are highly complex. The results also showed that MSE_{σ^2} values decrease with ageing and pathology [25].

EEG irregularity and complexity analyses have been successfully and widely employed and provide a new view to understand physiological processes in both healthy and pathological conditions in AD [1,11,13,26–28]. The MSE- and mvMSE-based methods have been successfully used to characterise biomedical signals to detect different pathological states like epilepsy, schizophrenia, Parkinson's disease, and AD [13,29–32].

Escudero et al. used multiscale entropy with a coarse-graining process based on the mean to characterise EEGs in AD [11]. Later, Morabito et al. analysed EEGs in AD patients with multivariate entropy techniques based on the mean [13]. However, since the dataset included few subjects and channels, the results may not be completely reliable [13]. Azami and colleagues used only mvMSE_{μ} for magnetoencephalograms (MEGs) in AD [32]. They consider five subsets of channels and not all the channels as a whole. Multiscale approaches using the variance in the coarse-graining process have yet to be applied to EEG analysis. Therefore, there is a need to investigate the usefulness of MSE_{σ^2} and mvMSE where the coarse graining process uses variance (mvMSE_{σ^2}) in comparison with the more broadly used methods based on mean (MSE_{μ} and mvMSE_{μ}) to characterise EEGs in AD.

The aim of this research is to investigate the first and second moments (mean and variance) for the coarse-graining process of MSE and mvMSE to characterise EEGs to discriminate age-matched control subjects from AD patients. We want to evaluate the differences between results obtained by the multiscale entropy methods and their corresponding multivariate versions. We also test the hypothesis that AD patients' signals are less complex than controls' recordings [13,19]. In addition, the changes in entropy values for different frequency bands are investigated to understand the effect of AD and entropy-based methods on each frequency band.

The outline of this paper is as follows. The next section describes the EEG data used in this study and explains briefly the MSE_{μ}, MSE_{σ^2}, mvMSE_{μ}, and mvMSE_{σ^2} algorithms. Results are presented in Section 3. The discussions and conclusions are explained in Sections 4 and 5, respectively.

2. Materials and Methods

2.1. Subjects

Eleven AD patients (five men; six women; age: 72.5 $\pm$ 8.3 years, mean $\pm$ standard deviation (SD)) and 11 age-matched control subjects (seven men; four women; age: 72.8 $\pm$ 6.1 years, mean $\pm$ SD) took part in this study. All 22 subjects were recruited from the Alzheimer's Patients' Relatives Association of Valladolid, Spain, and fulfilled the criteria of probable AD [33]. The EEG signals were recorded in the University Hospital of Valladolid, Spain, after all of the subjects had undergone a careful clinical assessment which included clinical history, neurological and physical examinations, brain scans and a mini mental state examination (MMSE), as a commonly accepted, simplified, scored form of the cognitive mental status examination [34].

The average of MMSE scores for the AD patients was 13.1 $\pm$ 5.9 points (mean $\pm$ SD), demonstrating that the mean of the disease degree is moderate, but five patients had an MMSE score below 12 points and, therefore, severe AD dementia. Two subjects were taking lorazepam at the time of the recording, which may improve the beta activity with therapeutic doses, although no prominent fast rhythms were seen in the visual inspection of their EEG signals. The other patients did not use any medication that could be expected to affect the EEG recordings [35,36]. The MMSE score value for 11 age-matched elderly control subjects without past or present neurological disorders was 30 $\pm$ 0. Informed consent was obtained for all 22 subjects and the local ethics committee approved the study.

2.2. EEG Recordings

More than 5 min of EEG time series were recorded from each subject with a Profile Study Room 2.3.411 EEG equipment (Oxford Instruments) at electrodes F3, F4, F7, F8, Fp1, Fp2, T3, T4, T5, T6, C3, C4, P3, P4, O1, O2, Fz, Cz, and Pz of the international 10–20 system with a linked ear lobes reference.

The signals have a sampling frequency of 256 Hz, with a 12-bit analog-to-digital precision. The EEGs from all 22 subjects were recorded when they were awake and eyes-closed to obtain less noisy signals. A specialist clinician selected 5 s epochs (1280 sample points) with minimal artefacts to be appropriately used for analysis. For each subject, 30.0 ± 12.5 (mean ± SD) artefact-free epochs were chosen from each electrode. Before analysis, all EEG time series were digitally band-pass filtered in both forward and reverse directions to avoid net phase shift with a Hamming window FIR filter of order 200 and cut-off frequencies at 1 Hz and 40 Hz to remove residual electromyographic activity.

2.3. Methods

2.3.1. Multiscale Entropy Based on Mean and Variance

MSE methods include two steps: (I) coarse-graining process and (II) calculation of SampEn at each scale factor.

(I) Assume we have a signal $\{x_1, x_2, \ldots, x_b, \ldots, x_C\}$ with length C. Each element of the coarse-grained time series for MSE_{μ} and recently proposed MSE_{σ^2} are respectively calculated as:

$$ {}^{\mu}y_i^{(\lambda)} = \frac{1}{\lambda} \sum_{b=(i-1)\lambda+1}^{i\lambda} x_b \qquad 1 \le i \le \left\lfloor \frac{C}{\lambda} \right\rfloor = N \tag{1} $$

$$ {}^{\sigma^2}y_i^{(\lambda)} = \frac{1}{\lambda} \sum_{b=(i-1)\lambda+1}^{i\lambda} \left(x_b - {}^{\mu}y_i^{(\lambda)}\right)^2 \qquad 1 \le i \le \left\lfloor \frac{C}{\lambda} \right\rfloor = N \tag{2} $$

where λ, $\mathbf{y} = \{y_1, y_2, \ldots, y_N\}$, and N denote the scale factor, the coarse-grained signal, and its length, respectively [17,25]. In fact, the coarse-grained time series of MSE_{μ} and MSE_{σ^2} are respectively the mean and variance values of consecutive sample points [17,25]. Note that the coarse-graining process based on the mean and variance start from scale factor 1 and 2, respectively [17,25].

(II) At each scale factor, the SampEn of the coarse-grained signal $\mathbf{y} = \{y_1, y_2, \ldots, y_N\}$ is calculated in the next step. For the sake of conciseness, here, we use y_i for both the coarse-grained signals ${}^{\sigma^2}y_i^{(\lambda)}$ and ${}^{\mu}y_i^{(\lambda)}$. At each time t of $\mathbf{y}$, a vector $Y_t^m = \{y_t, y_{t+1}, \ldots, y_{t+m-2}, y_{t+m-1}\}$ for $t = 1, 2, \ldots, N-(m-1)$, including the m-th subsequent values is constructed, where m, named embedding dimension, stands for how many samples are contained in each vector. Next, the distance between such vectors as the maximum difference of their corresponding scalar components, $d\left[Y_{t_1}^m, Y_{t_2}^m\right] = \max\left\{\left|Y_{t_1+k}^m - Y_{t_2+k}^m\right| : 0 \le k \le m-1 \text{ and } t_1 \ne t_2\right\}$ are calculated. A match happens when the distance $d\left[Y_{t_1}^m, Y_{t_2}^m\right]$ is smaller than a predefined tolerance r. The probability $B^m(r)$ shows the total number of m-dimensional matched vectors [15]. Similarly, $B^{m+1}(r)$ is defined for embedded dimension of $m+1$. Finally, the SampEn is defined as follows [15]:

$$ SampEn(y, m, r) = -\ln\left(B^{m+1}(r)/B^m(r)\right) \tag{3} $$

where m and r for SampEn were, respectively, chosen as 2, and 0.15 multiplied by the SD of the original time series following recommendations in [15].

2.3.2. Multivariate Multiscale Entropy Based on Mean and Variance

Like MSE, mvMSE includes two main steps: (I) coarse-graining process and (II) calculation of multivariate SampEn (mvSE) at each scale factor.

(I) Assume we have a p-channel (multivariate) time series $\mathbf{Z} = \left\{z_{q,b}\right\}_{b=1}^{C}$, $q = 1, \ldots, p$, where C is the length of each channel's signal. Each element of the coarse-grained time series is calculated as follows:

$$ {}^{\mu}u_{q,i}{}^{(\lambda)} = \frac{1}{\lambda} \sum_{b=(i-1)\lambda+1}^{i\lambda} z_{q,b} \qquad 1 \leq i \leq \left\lfloor \frac{C}{\lambda} \right\rfloor = N,\ 1 \leq q \leq p \tag{4} $$

where λ is the time scale factor [17,22,37]. As an extension of MSE_{σ^2} [25] to multi-channel signals, we propose to use variance, instead of mean value, in the coarse-graining process as follows:

$$ {}^{\sigma^2}u_{q,i}{}^{(\lambda)} = \frac{1}{\lambda} \sum_{b=(i-1)\lambda+1}^{i\lambda} \left(z_{q,b} - {}^{\mu}u_{q,i}{}^{(\lambda)}\right)^2 \qquad 1 \leq i \leq \left\lfloor \frac{C}{\lambda} \right\rfloor = N,\ 1 \leq q \leq p \tag{5} $$

(II) Second, for the defined scale factor λ, the mvSE of the coarse-grained signal is calculated [24,37,38]. To calculate the mvSE, multivariate embedded vectors are initially generated [24]. In [39], the Takens embedding theorem for multivariate concept is described. Using the p-channel signal $\mathbf{U} = \left\{u_{q,i}\right\}_{q=1,\ i=1}^{q=p,\ i=N}$ where N is the length of each coarse-grained time series $\left\{\mathbf{u}_q\right\}_{q=1}^{p}$, the multivariate embedded reconstruction is defined as:

$$ U_m(i) = [u_{1,i}, u_{1,i+\tau_1}, \ldots, u_{1,i+(m_1-1)\tau_1}, u_{2,i}, u_{2,i+\tau_2}, \ldots, u_{2,i+(m_2-1)\tau_2}, \ldots, u_{p,i}, u_{p,i+\tau_p}, \ldots, u_{p,i+(m_p-1)\tau_p}] \tag{6} $$

where $\mathbf{m} = [m_1, m_2, \ldots, m_p]$ and $\boldsymbol{\tau} = [\tau_1, \tau_2, \ldots, \tau_p]$ are the embedding and the time lag vectors, respectively.

For p-variate time series $\left\{\mathbf{u}_q\right\}_{q=1}^{p}$, the mvSE algorithm, as a natural extension of standard SampEn, is described as follows [24]:

1. Form multivariate embedded vectors $U_m(i) \in R^m$ where $i = 1, 2, \ldots, N-n$ and $n = max\{\mathbf{m}\} \times max\{\boldsymbol{\tau}\}$.
2. Calculate the distance between any two composite delay vectors $U_m(i)$ and $U_m(j)$ as the maximum norm.
3. For a given $U_m(i)$ and a threshold r, count the number of instances P_i where $d[U_m(i), U_m(j)] \leq r$, $i \neq j$. Next, calculate the frequency of occurrence as $\phi_i^m(r) = \frac{1}{N-n} P_i$ and define a global quantity $\phi^m(r) = \frac{1}{N-n} \sum_{i=1}^{N-n} \phi_i^m(r)$.
4. Extend the dimensionality of the multivariate delay vector in (6) from m to $(m+1)$ (keep the dimension of the other variables unchanged).
5. Repeat steps 1–4 and find $\phi_i^{(m_q+1)}(r)$. Next, calculate $\phi_i^{(m+1)}(r)$ which denotes the average over all n of $\phi_i^{(m_q+1)}(r)$. Finally, find $\phi_i^{(m+1)}(r)$ which stands for the average over all i of $\phi_i(r)$ in an $(m+1)$-dimensional space.
6. Finally, mvSE is defined as:

$$ mvSE(\mathbf{Z}, \mathbf{m}, \boldsymbol{\tau}, r) = -\ln\left(\frac{\phi^{(m+1)}(r)}{\phi^m(r)}\right) \tag{7} $$

where m_k, τ_k, and r for all of the approaches were, respectively, chosen as 2, 1, and 0.15 multiplied by the SD of the original time series according to [15,24]. Note that the number of sample points is at least 10^m, or preferably at least 30^m, to robustly estimate SampEn and mvSE, according to [24,40,41].

Since multivariate time series may have different amplitude ranges, the distances calculated from embedded vectors obtained with Takens embedding theorem may be dominated by components of the vectors coming from the time series with the largest amplitudes. Thus, we scale all of the data channels to the same amplitude range and normalise each data channel to unit SD so that the total variation becomes equal to the number of channels or variables [24].

2.4. Experimental Procedures

In addition to the original EEG signals band-pass filtered between 1 Hz and 40 Hz, we investigate the MSE_{μ}, mvMSE_{μ}, MSE_{σ^2}, and mvMSE_{σ^2} on different EEG frequency bands, including θ, α, and β. Note that δ and γ, respectively, have too low and high frequency to be considered here based on the fact that the MSE_{μ} and mvMSE_{μ} methods at scale factor λ can be considered as a low-pass filter with cut-off frequency $\frac{f_s}{2\lambda}$ [42].

Another powerful strategy to discriminate the controls from AD subjects is to use the slope values as features of the MSE and mvMSE profiles [11]. The MSE and mvMSE profiles, showing, respectively, the SampEn and mvSE values of each coarse-grained time series versus the scale factor, were visually inspected to determine the range of scales over which the slope would be calculated. A nonparametric test, namely the Mann–Whitney *U*-test, was used to evaluate the differences between results for AD patients versus controls, as the entropy values at each scale factor did not follow a normal distribution. The scales with the *p*-values between 0.01 and 0.05 (significant), and less than 0.01 (very significant) are shown with + and *, respectively, in this study.

3. Results

3.1. Global Evaluation of Multivariate and Univariate Multiscale Entropies

The results obtained by the MSE_{μ}, mvMSE_{μ}, MSE_{σ^2}, and mvMSE_{σ^2} methods are, respectively, shown in Figures 1–4. For each of Figures 1–4, (a)–(d) show the results at frequency bands 1–40 Hz, θ, α, and β, respectively. As can be seen in (b)–(d) of Figures 1–4, the results obtained at frequency bands θ, α, and β do not show that controls' signals are more complex than AD patients' ones. This fact suggests that complexity changes are best highlighted considering broadband activity.

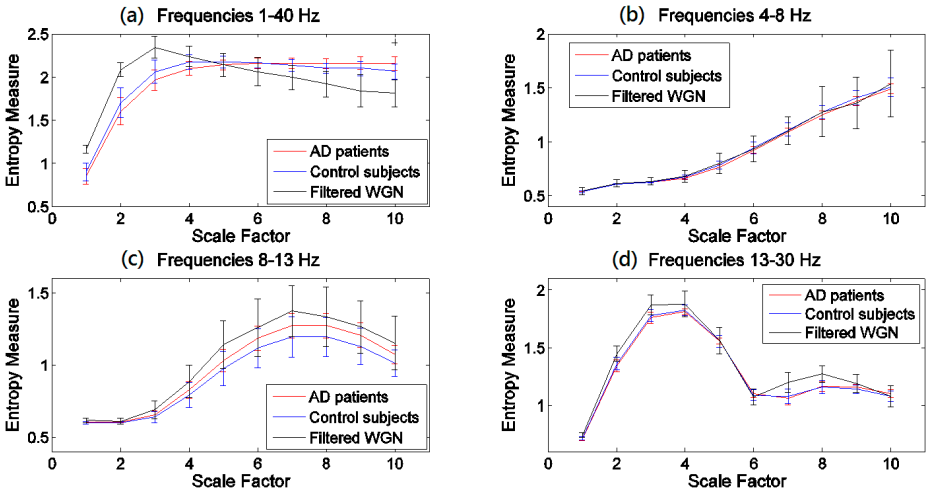

Figure 1. Plots illustrating the mean ± SD (as error bars) of the MSE_{μ} values computed from 11 AD, 11 control subjects' signals, and 40 filtered univariate WGN time series at frequency bands (**a**) 1–40 Hz; (**b**) θ (4–8 Hz); (**c**) α (8–13 Hz); and (**d**) β (13–30 Hz). The scales with the *p*-values between 0.01 and 0.05, and less than 0.01, are shown with + and *, respectively.

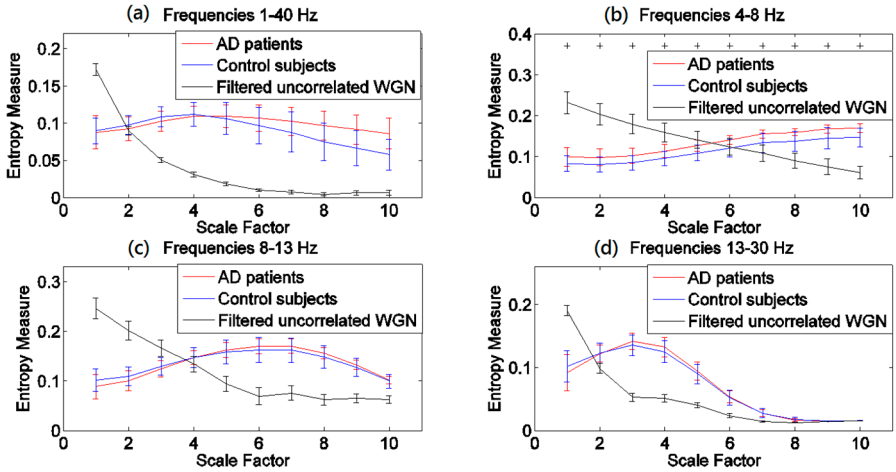

Figure 2. Plots illustrating the mean ± SD (as error bars) of the mvMSE_{μ} values computed from 11 AD, 11 control subjects' signals, and 40 filtered uncorrelated sixteen-channel WGN time series at frequency bands (**a**) 1–40 Hz; (**b**) θ (4–8 Hz); (**c**) α (8–13 Hz); and (**d**) β (13–30 Hz). The scales with the p-values between 0.01 and 0.05, and less than 0.01, are shown with + and *, respectively.

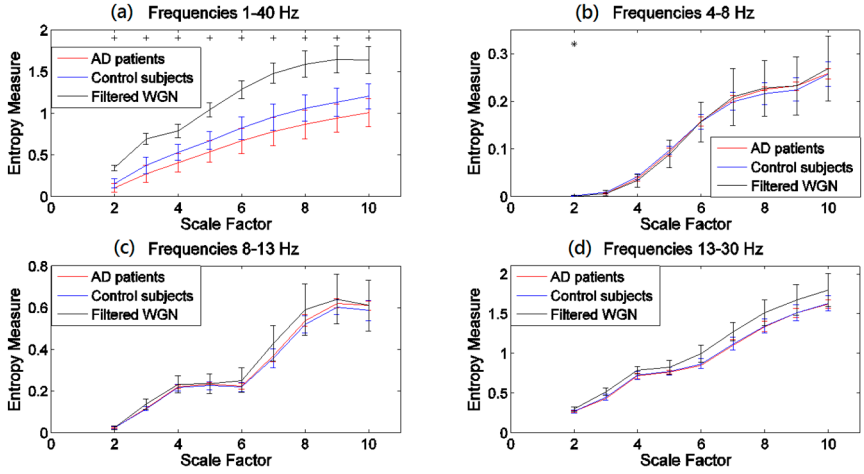

Figure 3. Plots illustrating the mean ± SD (as error bars) of the MSE_{σ^2} values computed from 11 AD, 11 control subjects' signals, and 40 filtered univariate WGN time series at frequency bands (**a**) 1–40 Hz; (**b**) θ (4–8 Hz); (**c**) α (8–13 Hz); and (**d**) β (13–30 Hz). The scales with the p-values between 0.01 and 0.05, and less than 0.01, are shown with + and *, respectively.

In Figures 1a and 2a, the profiles of the mvMSE_{μ} and mvMSE_{μ} are different for the control individuals and AD patients at short- and long-time scale factors. In comparison with the AD group, controls' signals have more irregularity at short-time scales, whereas the AD patients' time series are more irregular at long-time scales.

Comparing Figure 1 with Figure 2 demonstrates that mvMSE_{μ} highlights differences between groups at individual scales better than the averaging of univariate MSE_{μ} profiles. However, the opposite seems to happen for MSE_{σ^2} (Figure 3) when compared with mvMSE_{σ^2} (Figure 4). This might be because the variance coarse-grained sequences have too little variability and the multivariate implementation leads to values that are too low (notice that the output values are in 1/100s of the unit).

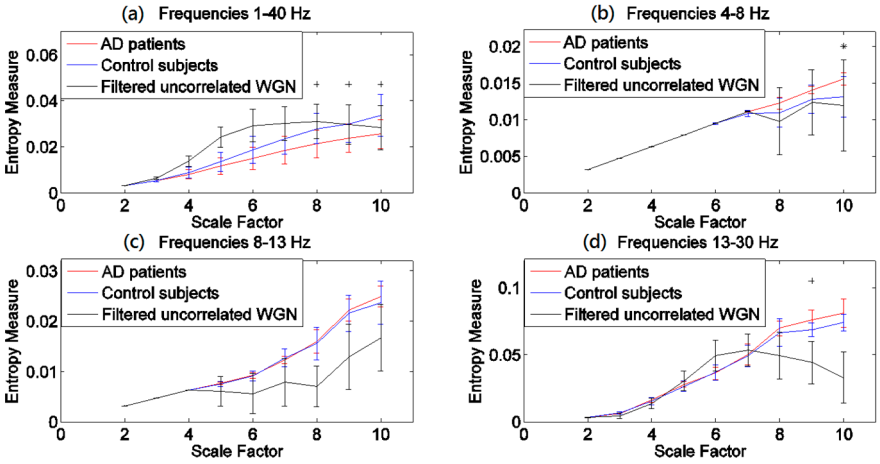

Figure 4. Plots illustrating the mean ± SD (as error bars) of the mvMSE_{σ^2} values computed from 11 AD, 11 control subjects' signals, and 40 filtered uncorrelated sixteen-channel WGN time series at frequency bands (**a**) 1–40 Hz; (**b**) θ (4–8 Hz); (**c**) α (8–13 Hz); and (**d**) β (13–30 Hz). The scales with the p-values between 0.01 and 0.05, and less than 0.01, are shown with + and *, respectively.

The results obtained using the variance-based coarse graining process (Figures 3a and 4a), unlike the mean-based ones (Figures 1a and 2a), show that for all the scale factors, the controls' EEGs have a higher complexity. This is in agreement with findings that controls' time series are more complex than AD patients' [11,19,25,32,35,38,43,44]. Of note is that the ranges of entropy values for Figures 1 and 2, and similarly Figures 3 and 4, indicate that the larger the number of channels, the smaller the multivariate entropy values. For more information, please refer to Appendix A.

The p-values for MSE_{σ^2}- and mvMSE_{σ^2}-based profiles show that MSE_{σ^2} leads to significant differences at all scale factors, while the significant differences based on mvMSE_{σ^2} are seen at scale factors 8 and 10. In comparison with MSE_{μ}, MSE_{σ^2} discriminates better AD group and controls, while compared with mvMSE_{σ^2}, mvMSE_{μ} discriminates better these two groups. It shows that the mean- and variance-based complexity measures can complement each other to characterise EEGs in AD. It is worth noting that the results obtained by different values of r (0.2, 0.25, and 0.3) and m (1 and 2) employed in other complexity studies are similar to our results [11,32,44,45].

Note that all channels are considered as a multivariate whole for multivariate entropy techniques although for the univariate ones, the entropy value is computed for each channel. Since the average is reported for MSE-based methods, the results are probably expected to have lower coefficients of variations, although these methods cannot take into account the dynamics across the channels (spatial domain).

In the light of a recently published article providing guidelines on the interpretation of MSE_{μ} results of brain signals [46], we evaluated all MSE and mvMSE methods on 40 different univariate and uncorrelated multivariate WGN time series band-pass filtered at 1–40 Hz, 4–8 Hz, 8–13 Hz, and 13–30 Hz, to investigate whether the entropy profiles of brain signals are linked to their power content. The length of the time series and the number of channels of the filtered multivariate WGN were respectively 1280 sample points (equal to the length of the EEG time series) and 16 (equal to the number of channels of EEG time series), and the parameter values for the multiscale methods were equal to those used for the EEG dataset. The results, shown in Figures 1–4, show that the shape of MSE_{μ} and MSE_{σ^2} curves are linked to the power spectral density of the corresponding filtered signals. In fact, to some extent, the MSE curves are determined by the (low and high cut-offs of the) filtering process, especially for frequency bands 4–8 Hz, 8–13 Hz, and for 13–30 Hz to a lesser extent. However, it is important to note that the entropy profiles for EEG signals of AD patients and controls do not overlap with the curves of the filtered WGN at most scale factors for the frequency band of 1–40 Hz. It also evidences the need to have broadband EEGs, instead of narrow band activity, for the

evaluation of multiscale complexity. In contrast with the results of univariate entropy techniques, the $mvMSE_{\mu}$- and $mvMSE_{\sigma^2}$-based curves for AD patients and controls have clearly dissimilar shapes with those for filtered uncorrelated multichannel WGN, suggesting that the multivariate entropy-based values of AD patients' and controls' time series are completely different to those of filtered uncorrelated sixteen-channel WGN.

The computation times of the MSE_{μ}, $mvMSE_{\mu}$, MSE_{σ^2}, and $mvMSE_{\sigma^2}$ methods for one of the 16-channel AD signals with the length of 1280 sample points are shown in Table 1. Note that the running time for the MSE-methods is the sum of computation time values for each of the 16 channels. In this study, the simulations have been carried out using a PC with Intel (R) Xeon (R) CPU, E5420, 2.5 GHz and 8-GB RAM by MATLAB R2010a. Since the MSE_{σ^2} and $mvMSE_{\sigma^2}$ start from scale factor 2 and SampEn has a computational cost of $O(N^2)$, the computation time of this kind of algorithms is noticeably smaller than that of the MSE_{μ} or $mvMSE_{\mu}$ algorithms. The mvMSE methods deal with both the spatial and time domains, albeit the MSE algorithms consider only the time domain. Thus, as can be seen in Table 1, the MSE techniques are significantly faster than their corresponding mvMSE methods.

Table 1. The computation time of the univariate and multivariate multiscale entropy based on the mean and variance.

MSE_{μ}	$mvMSE_{\mu}$	MSE_{σ^2}	$mvMSE_{\sigma^2}$
4.77 s	21.78 s	2.4 s	8.05 s

3.2. Regional Evaluation with Univariate Metrics

To evaluate the complexity of the signal of each channel of AD patients' and controls' EEGs, we employ univariate MSE methods. The MSE_{μ} and MSE_{σ^2} values and their p-values for each channel of EEGs, band-pass-filtered between 1 and 40 Hz, are presented in Figures 5 and 6, respectively. The p-values show the superiority of MSE_{σ^2} over MSE_{μ} for characterising AD. Moreover, the lowest p-values for MSE_{σ^2} that obtained by the channels O1, O2, and P3 were equal to 0.0058, 0.0086, and 0.0087, respectively, in agreement with [11].

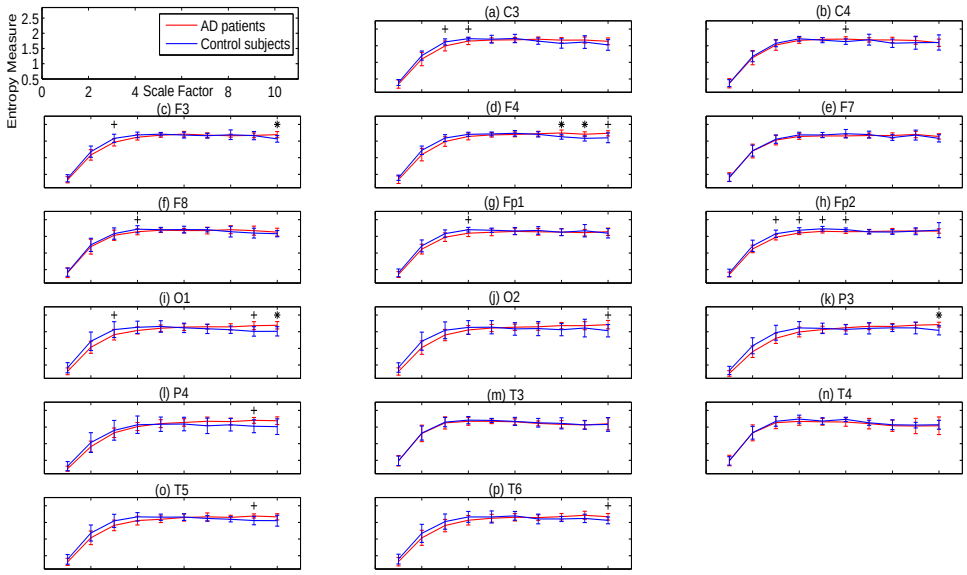

Figure 5. Plots illustrating the mean ± SD (as error bars) of the MSE_{μ} values computed from 11 AD and 11 control subjects for each channel of 1–40 Hz band-pass-filtered EEG signals. Sixteen electrodes of the international 10–20 system were analysed. (**a**) C3; (**b**) C4; (**c**) F3; (**d**) F4; (**e**) F7; (**f**) F8; (**g**) Fp1; (**h**) Fp2; (**i**) O1; (**j**) O2; (**k**) P3; (**l**) P4; (**m**) T3; (**n**) T4; (**o**) T5; and (**p**) T6. The scales with the p-values between 0.01 and 0.05, and less than 0.01 are shown with + and *, respectively.

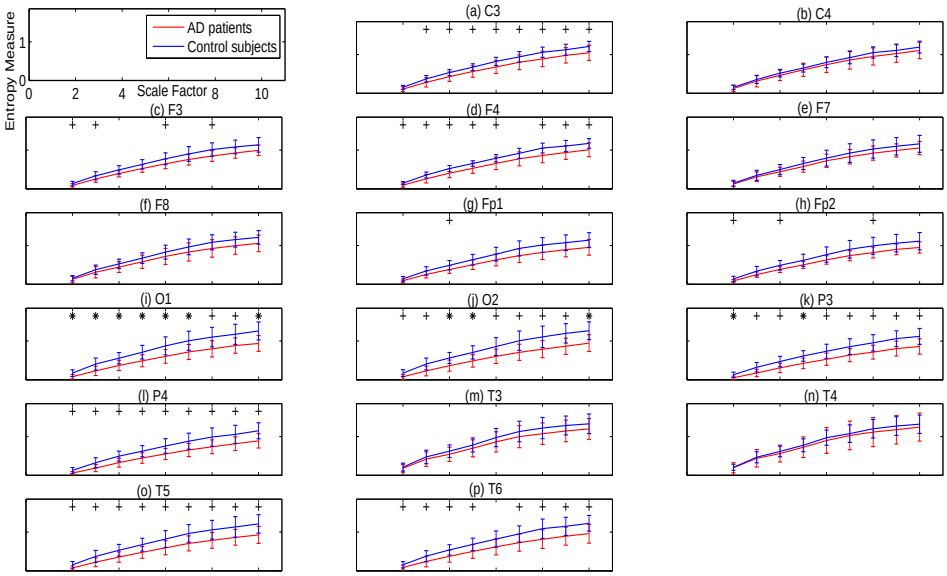

Figure 6. Plots illustrating the mean ± SD (as error bars) of the MSE_{σ^2} values computed from 11 AD and 11 control subjects for each channel of 1–40 Hz bandpass filtered EEG signals. Sixteen electrodes of the international 10–20 system were analysed. (**a**) C3; (**b**) C4; (**c**) F3; (**d**) F4; (**e**) F7; (**f**) F8; (**g**) Fp1; (**h**) Fp2; (**i**) O1; (**j**) O2; (**k**) P3; (**l**) P4; (**m**) T3; (**n**) T4; (**o**) T5; and (**p**) T6. The scales with the *p*-values between 0.01 and 0.05, and less than 0.01 are shown with + and *, respectively.

3.3. Features (Slopes) from Univariate and Multivariate Multiscale Profiles

As mentioned before, a powerful strategy to distinguish different kinds of dynamics consists in using the slopes as features from multivariate and univariate multiscale entropy profiles. As can be seen in Figures 1a and 2a, for MSE_{μ} and $mvMSE_{\mu}$ methods, the curves increase until a scale factor of 4. Then, the slope decreases and the SampEn and mvSE values are nearly constant or decrease slightly. Therefore, we can divide each of the MSE and mvMSE curves into two segments: (I) the first part corresponds to the steep increasing slope (small scale factors, i.e., $1 \leq \lambda \leq 4$), and (II) the second one contains the scale factors in which the slope of the SampEn and mvSE values is smoother (large scale factors, i.e., $5 \leq \lambda \leq 10$). For MSE_{σ^2} and $mvMSE_{\sigma^2}$ profiles, because the curves are always ascending and their slope values do not change noticeably, we consider one slope from the scale factor 2–10 (the entropy values for MSE_{σ^2} and $mvMSE_{\sigma^2}$ methods are undefined at a scale factor of 1). Note that the slope values of both parts were calculated based on the least-square approach.

Table 2 shows the average ± SD of slope values of the MSE and mvMSE profiles for small and large time scales. We also calculate the *p*-values of the Mann–Whitney *U*-test to investigate whether there is any significant difference between the AD and control groups. Like Figures 1–6, the scales with the *p*-values between 0.01 and 0.05, and less than 0.01, are denoted by + and *, respectively. For small scale factors, no significant differences between both groups can be found with the MSE_{μ} and $mvMSE_{\mu}$, whereas the differences between these groups are significant (MSE_{μ}) and very significant ($mvMSE_{\mu}$) when we consider the large scale factors. This demonstrates the importance of mvMSE method to characterise EEG signals in AD. Moreover, both the MSE_{σ^2} and $mvMSE_{\sigma^2}$ methods lead to the significant differences for AD patients and controls.

The slopes were also computed for each channel to investigate which channels discriminate better the two subject groups. All results at scale factors $1 \leq \lambda \leq 4$ did not lead to significant differences. Table 3 summarises the average ± SD of slope values of the MSE_{μ} profiles with scale factors $5 \leq \lambda \leq 10$. Table 3 also shows that the *p*-values for all channels at large scale factors leads to (very) significant differences for several channels. The average ± SD of slope values for MSE_{σ^2} curves are shown in Table 4. The *p*-values derived by electrodes O1, O2, F4, P3, and T5 for both the MSE_{μ} with scale factors

$5 \leq \lambda \leq 10$ and MSE_{σ^2} profiles are (very) significant. The p-values for F4 and O1 are smaller than 0.05 for MSE_{μ} with scale factors $5 \leq \lambda \leq 10$, while electrode O2 leads to the significant difference using the MSE_{σ^2} method. This suggests that variance- and mean-based MSE offer complementary approaches to characterise AD.

Table 2. Average ± SD of slope values of the MSE and mvMSE profiles, and p-values and classification accuracies for AD patients versus controls over all channels and subjects. The scales with the p-values between 0.01 and 0.05, and less than 0.01 are shown with $^+$ and *, respectively.

Method	AD Patients	Controls	p-Value	Classification Ratio
MSE_{μ} $(1 \leq \lambda \leq 4)$	0.4107 ± 0.0226	0.4185 ± 0.0238	0.3933	63.64%
MSE_{μ} $(5 \leq \lambda \leq 10)$ $_+$	0.0022 ± 0.0195	-0.0216 ± 0.0240	0.0215	72.73%
MSE_{σ^2} $(2 \leq \lambda \leq 10)$ $^+$	0.1130 ± 0.0154	0.1301 ± 0.0137	0.0151	72.73%
$mvMSE_{\mu}$ $(1 \leq \lambda \leq 4)$	0.0074 ± 0.0088	0.0077 ± 0.0092	0.5114	31.82%
$mvMSE_{\mu}$ $(5 \leq \lambda \leq 10)$ *	-0.0048 ± 0.0037	-0.0099 ± 0.0033	0.0071	72.73%
$mvMSE_{\sigma^2}$ $(2 \leq \lambda \leq 10)$ $^+$	0.0030 ± 0.0009	0.0041 ± 0.0012	0.0302	63.64%

Table 3. Average ± SD of slope values of the MSE_{μ} profiles and p-values for controls versus AD patients at scale factors $(5 \leq \lambda \leq 10)$ for each channel. The scales with the p-values between 0.01 and 0.05, and less than 0.01 are shown with $^+$ and *, respectively.

Electrode	AD Patients	Controls	p-Value
C3	-0.006 ± 0.0302	-0.0360 ± 0.0356	0.0762
C4	-0.018 ± 0.0264	-0.0160 ± 0.0472	0.8955
F3	-0.001 ± 0.0171	-0.0209 ± 0.0238	0.0878
F4 *	0.0076 ± 0.0244	-0.0318 ± 0.0220	0.0031
F7	0.0018 ± 0.0219	-0.0206 ± 0.0317	0.1150
F8 $^+$	-0.007 ± 0.0285	-0.0279 ± 0.0149	0.0418
Fp1	-0.001 ± 0.0174	-0.0136 ± 0.0443	0.1007
Fp2	0.0029 ± 0.0115	-0.0099 ± 0.0378	0.0660
O1 *	0.0162 ± 0.0285	-0.0306 ± 0.0256	0.0031
O2 $^+$	0.0194 ± 0.0277	-0.0136 ± 0.0415	0.0418
P3 $^+$	0.0276 ± 0.0238	-0.0040 ± 0.0453	0.0488
P4	0.0177 ± 0.0303	-0.0151 ± 0.0399	0.0660
T3	-0.019 ± 0.0379	-0.0267 ± 0.0390	0.8438
T4	-0.029 ± 0.0496	-0.0324 ± 0.0297	0.7427
T5 $^+$	0.0139 ± 0.0278	-0.0246 ± 0.0312	0.0126
T6	0.0120 ± 0.0361	-0.0213 ± 0.0494	0.0660

Table 4. Average ± SD of slope values of the MSE_{σ^2} profiles and p-values for controls versus AD patients at scale factors $(\lambda \leq 10)$ for each channel. The scales with the p-values between 0.01 and 0.05, and less than 0.01 are shown with $^+$ and *, respectively.

Electrode	AD Patients	Controls	p-Value
C3 $^+$	0.1163 ± 0.0178	0.1296 ± 0.0119	0.0488
C4	0.1213 ± 0.0186	0.1289 ± 0.0135	0.2643
F3	0.1127 ± 0.0127	0.1257 ± 0.0173	0.0660
F4 $^+$	0.1139 ± 0.0164	0.1278 ± 0.0123	0.0418
F7	0.1161 ± 0.0133	0.1273 ± 0.0204	0.1891
F8	0.1165 ± 0.0183	0.1326 ± 0.0154	0.0569
Fp1	0.1079 ± 0.0212	0.1253 ± 0.0182	0.1486
Fp2	0.1085 ± 0.0148	0.1226 ± 0.0214	0.1310
O1 $^+$	0.1080 ± 0.0186	0.1342 ± 0.0208	0.0126
O2 *	0.1078 ± 0.0195	0.1358 ± 0.0219	0.0071
P3 $^+$	0.1023 ± 0.0193	0.1231 ± 0.0183	0.0356
P4 $^+$	0.1038 ± 0.0180	0.1255 ± 0.0201	0.0215
T3	0.1267 ± 0.0218	0.1406 ± 0.0201	0.1486
T4	0.1301 ± 0.0314	0.1389 ± 0.0210	0.4307
T5 $^+$	0.1069 ± 0.0203	0.1307 ± 0.0215	0.0418
T6 $^+$	0.1091 ± 0.0216	0.1327 ± 0.0187	0.0256

We also classified the controls versus AD subjects using a naive Bayes method [47]. The slope values across the scale factors were used rather than the entropy values of all scale factors, because a slope value can be considered as a representative value of a complexity-based curve [11]. We ran 50 repetitions of a 10-fold cross-validation using the WEKA data mining software [48]. The average classification values are reported in Table 2. As expected intuitively, the highest and lowest classification accuracies are associated with the largest and smallest p-values, respectively.

4. Discussion and Conclusions

4.1. Global Evaluation of Multivariate and Univariate Multiscale Entropies

We compared the ability of MSE_{μ}, $mvMSE_{\mu}$, MSE_{σ^2}, and $mvMSE_{\sigma^2}$ to characterise the complexity of EEG signals in AD. This was done for conventional frequency bands θ, α, and β, and also for the broadband EEG signals after band-pass filtering between 1 and 40 Hz. The results obtained for frequency bands θ, α, and β were in contradiction with the widely reported higher complexity in control subjects than in AD patients, which could nevertheless be observed when estimating the complexity of the broadband EEGs. This suggests that the presence of broadband activity of EEGs may be needed for a comprehensive evaluation of complexity with multiscale entropy-based methods. Furthermore, we have related these findings with a very recent article providing guidelines on the interpretation of MSE results of brain signals [46] and showed that the profile of multivariate multiscale entropy of EEG signals at different frequency bands is not determined by the band-pass filtering process in comparison with the univariate multiscale entropy.

For the MSE_{μ} and $mvMSE_{\mu}$ curves, the slope of the curve increasing or decreasing at different bands can be predicted based on the sampling frequency and the effect of coarse-graining process on the frequency of signals. Since MSE_{μ} and $mvMSE_{\mu}$ at scale factor λ can be considered as a low-pass filter with cut-off frequency $\frac{f_s}{2\lambda}$ [42], scales 9 and 10, and 4–10 of the broadband analysis corresponds with α and β, respectively, with θ falling off the range.

The $mvMSE_{\mu}$-based profiles (Figure 2a) were similar to MSE_{μ}-based ones (Figure 1a), although the crossing point for $mvMSE_{\mu}$ results was located at a smaller scale factor compared with that obtained by MSE_{μ}. These results are in agreement with [11,32,35,38,43,44]. Unlike MSE_{μ} and $mvMSE_{\mu}$, MSE_{σ^2}, and $mvMSE_{\sigma^2}$ of the controls' EEGs had more complexity values at all scale factors and smaller p-values. This suggests that both the multivariate and univariate multiscale methods based on the variance may characterise changes in EEGs in AD patients in a more detailed way than methods based on the mean.

The irregularity or complexity decrease in the EEG signals of AD patients could be described by a reduction of dynamical complexity of part of the brain [45]. Nevertheless, the pathophysiological implications of the reduction of EEGs complexity or irregularity are not quite clear. Among others, three mechanisms can take into account it: neuronal death, a general effect of lack of neurotransmitter, and loss of connectivity of local neural networks as a consequence of nerve cell death [12,49]. However, ageing and age-dependent diseases frequently go together with a broad-ranging loss of physiological complexity or irregularity [50].

4.2. Regional Evaluation with Univariate Metrics

The mvMSE methods reveal the dynamics across the channels and consider the information in both the time and spatial domains, while the MSE approaches only consider the time domain. However, the MSE methods, unlike the mvMSE algorithms, can be used to better understand the behaviour of each channel separately, which could highlight complexity changes that are specific to certain electrodes. To this end, we employed MSE_{σ^2} and MSE_{μ} to characterise EEGs in each channel. The lowest p-values for MSE_{σ^2} and MSE_{μ} were obtained for the channels O1, O2, P3, and P4 and O1, P3, F3, and F4, respectively. This shows that when MSE_{μ} (or $mvMSE_{\mu}$) cannot distinguish different types of dynamics of a particular time series (channel), MSE_{σ^2} (or $mvMSE_{\sigma^2}$) may do so, and vice

versa. It is worth noting that the electrodes with the lowest *p*-values are similar to most of our previous research using this database, such as [36,51].

4.3. Features (Slopes) from Univariate and Multivariate Multiscale Profiles

Finally, we studied the slope values of MSE and mvMSE profiles to check whether they could be used to distinguish AD patients from controls. The *p*-values for the slopes of the complexity curves showed the importance of this tool to discriminate different kinds of dynamics and demonstrated when the differences between AD patients' and controls' signals at some scale factors are not significant, their slopes of complexity curves may lead to significant differences. At small scale factors, significant differences were not found with the mean coarse-gaining-based approaches, while the differences between these groups were significant (MSE_{μ}) and very significant ($mvMSE_{\mu}$) when the large scale factors were considered. This also illustrates the prominence of the $mvMSE_{\mu}$ approach over MSE_{μ}. In addition, significant differences between AD patients and controls were found with both the MSE_{σ^2} and $mvMSE_{\sigma^2}$. The *p*-values at electrodes O1, O2, F4, P3, and T5 for both the MSE_{μ} and MSE_{σ^2} were significant or very significant.

4.4. Limitations

In spite of the promising results aforementioned, the number of subjects in this pilot study was relatively small. To ascertain the usefulness of these methods, these novel signal processing approaches should be used on a larger database of AD patients and controls subjects, potentially including subjects with mild cognitive impairment. Moreover, the subjects had their eyes closed during the recording of the EEG signals to obtain less noisy signals. However, the eyes closed condition increases frequency content in the alpha range. This increase could have induced a bias in the findings, especially when the alpha range was specifically studied. Thus, investigations under the eyes open condition are also required. In addition, the detected regularity increase in the EEG might not be exclusive to AD and supplementary work should be carried out to analyse whether these EEG complexity changes also happen in other types of dementia. The area under the complexity profiles is another potential feature of interest for future studies. Finally, a comprehensive comparison among all employed non-linear techniques should be done in the future.

5. Conclusions

In this pilot study, the ability of MSE_{μ}, $mvMSE_{\mu}$, MSE_{σ^2}, and $mvMSE_{\sigma^2}$ to characterise the complexity of different frequency bands of EEG signals in AD was investigated. MSE_{μ} and $mvMSE_{\mu}$, MSE_{σ^2}, and $mvMSE_{\sigma^2}$ quantify the dynamical properties of average and spread, respectively, over multiple time scales. They extract different kinds of information from signals. The results indicated that when MSE_{μ} or $mvMSE_{\mu}$ cannot distinguish different types of dynamics of a particular time series, MSE_{σ^2} or $mvMSE_{\sigma^2}$ may do so, and vice versa. The multivariate entropy methods may lead to more significant differences between groups by taking into account both the spatial and time domains. However, they cannot characterise the multivariate time series for single channels. Our results also evidenced that the presence of broadband activity in EEGs is required for a comprehensive evaluation of complexity with univariate and multivariate multiscale entropy approaches. From a clinical perspective, MSE_{σ^2} and $mvMSE_{\sigma^2}$ results were associated with a loss of complexity in AD time series and showed that the variance-based MSE and mvMSE better discriminate the AD patients' signals from the controls' ones in comparison with mean-based multiscale methods. The *p*-values for the slope values of mvMSE curves were smaller than for MSE, showing the possible usefulness of multivariate approaches. Overall, our results support the relevance of multivariate and univariate multiscale complexity analyses for the characterisation of EEG signals in AD.

Acknowledgments: We would like to thank Pedro Espino (Hospital Clinico San Carlos, Madrid, Spain) for his help in the recording and selection of EEG epochs.

Author Contributions: Hamed Azami and Javier Escudero conceived and designed the methodology. Hamed Azami was responsible for analysing and writing the paper. Daniel Abásolo, Samantha Simons, and Javier Escudero contributed critically to revise the results and discussed them. All authors have read and approved the final manuscript.

Conflicts of Interest: The authors declare no conflict of interest.

Appendix A

Sample entropy and multivariate sample entropy are used in the second step of the algorithms to quantify the complexity of univariate and multivariate time series, respectively. Sample entropy is based on the conditional probability that sequences close to each other for m consecutive data points will also be close to each other when one more point is added to each sequence. Thus, the proportion of unseen, new samples over the number of samples included in the previous pattern for the embedding dimension $m = 2$ is 50%. However, in multivariate sample entropy, multivariate embedded vectors are initially generated with the length of $m_1 + m_2 + ... + m_p$, where p denotes the number of channels of a time series. For example, for a trivariate time series with the embedding dimension $\mathbf{m} = [2, 2, 2]$, the length of embedded vectors is 6. Then, the conditional probability that sequences with the embedding dimension $\mathbf{m} = [2, 2, 2]$ close to each other for six data points will also be close to each other for seven data points, associated with the embedding dimensions [2, 2, 3], [2, 3, 2], or [3, 2, 2], is calculated. Note that the length of the newly embedded vectors is 7. Therefore, the proportion of unseen samples over the number of total samples in previous patterns for the embedding dimension $\mathbf{m} = [2, 2, 2]$ is 16.66%. Likewise, for a four-channel time series with the embedding dimension $\mathbf{m} = [2, 2, 2, 2]$, the proportion of unseen samples over the number of samples of previous patterns is 12.5%. Consequently, the proportion of new samples decreases proportionally to the number of channels, thus decreasing the likelihood of the longer new pattern not being a match with the shorter ones.

To investigate the changes in multivariate entropy values when the number of channels increases, we used an uncorrelated multivariate WGN time series that the number of its channels changes from 1 to 16 and the length of each of them is 1280 samples (equal to the length of EEG time series). Figure A1 shows how the number of channels affects the mvMSE output values. It can be seen that the larger the number of channels, the smaller the multivariate entropy values, something that agrees with our results, where the multivariate measures result in lower entropy values.

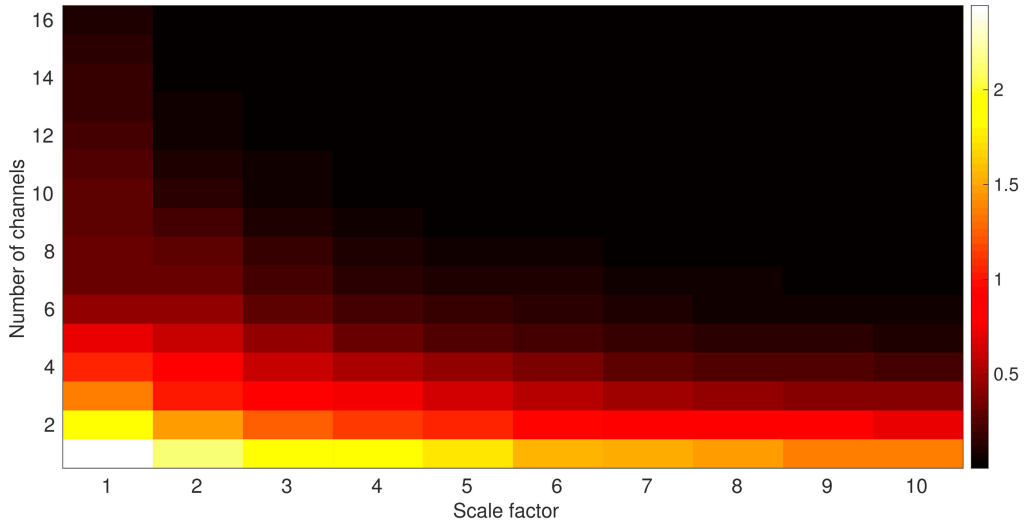

Figure A1. Multivariate Multiscale entropy values for the uncorrelated 1- to 16-channel WGN noise time series.

References

1. Bhat, S.; Acharya, U.R.; Dadmehr, N.; Adeli, H. Clinical neurophysiological and automated EEG-based diagnosis of the Alzheimer's disease. *Eur. Neurol.* **2015**, *74*, 202–210. [CrossRef] [PubMed]
2. Dauwels, J.; Vialatte, F.; Cichocki, A. Diagnosis of Alzheimer's disease from eeg signals: Where are we standing? *Curr. Alzheimer Res.* **2010**, *7*, 487–505. [CrossRef] [PubMed]
3. Alzheimer's Association. 2016 Alzheimer's disease facts and figures. *Alzheimers Dement.* **2016**, *12*, 459–509.
4. Sanei, S. *Adaptive Processing of Brain Signals*; John Wiley & Sons: Hoboken, NJ, USA, 2013.
5. Stam, C. Use of magnetoencephalography (MEG) to study functional brain networks in neurodegenerative disorders. *J. Neurol. Sci.* **2010**, *289*, 128–134. [CrossRef] [PubMed]
6. Hornero, R.; Escudero, J.; Fernández, A.; Poza, J.; Gómez, C. Spectral and nonlinear analyses of MEG background activity in patients with Alzheimer's disease. *IEEE Trans. Biomed. Eng.* **2008**, *55*, 1658–1665. [CrossRef] [PubMed]
7. Van der Hiele, K.; Vein, A.; Reijntjes, R.; Westendorp, R.; Bollen, E.; Van Buchem, M.; Van Dijk, J.; Middelkoop, H. EEG correlates in the spectrum of cognitive decline. *Clin. Neurophysiol.* **2007**, *118*, 1931–1939. [CrossRef] [PubMed]
8. Czigler, B.; Csikós, D.; Hidasi, Z.; Gaál, Z.A.; Csibri, É.; Kiss, É.; Salacz, P.; Molnár, M. Quantitative EEG in early Alzheimer's disease patients—Power spectrum and complexity features. *Int. J. Psychophysiol.* **2008**, *68*, 75–80. [CrossRef] [PubMed]
9. Moretti, D.; Fracassi, C.; Pievani, M.; Geroldi, C.; Binetti, G.; Zanetti, O.; Sosta, K.; Rossini, P.; Frisoni, G. Increase of theta/gamma ratio is associated with memory impairment. *Clin. Neurophysiol.* **2009**, *120*, 295–303. [CrossRef] [PubMed]
10. Andrzejak, R.G.; Lehnertz, K.; Mormann, F.; Rieke, C.; David, P.; Elger, C.E. Indications of nonlinear deterministic and finite-dimensional structures in time series of brain electrical activity: Dependence on recording region and brain state. *Phys. Rev. E* **2001**, *64*, 061907. [CrossRef] [PubMed]
11. Escudero, J.; Abásolo, D.; Hornero, R.; Espino, P.; López, M. Analysis of electroencephalograms in Alzheimer's disease patients with multiscale entropy. *Physiol. Meas.* **2006**, *27*, 1091. [CrossRef] [PubMed]
12. Jeong, J. EEG dynamics in patients with Alzheimer's disease. *Clin. Neurophysiol.* **2004**, *115*, 1490–1505. [CrossRef] [PubMed]
13. Labate, D.; La Foresta, F.; Morabito, G.; Palamara, I.; Morabito, F.C. Entropic measures of EEG complexity in Alzheimer's disease through a multivariate multiscale approach. *IEEE Sens. J.* **2013**, *13*, 3284–3292. [CrossRef]
14. Rostaghi, M.; Azami, H. Dispersion entropy: A measure for time series analysis. *IEEE Signal Process. Lett.* **2016**, *23*, 610–614. [CrossRef]
15. Richman, J.S.; Moorman, J.R. Physiological time-series analysis using approximate entropy and sample entropy. *Am. J. Physiol. Heart Circ. Physiol.* **2000**, *278*, H2039–H2049. [PubMed]
16. Sanei, S.; Chambers, J. *EEG Signal Processing*; John Wiley & Sons: Hoboken, NJ, USA, 2008.
17. Costa, M.; Goldberger, A.L.; Peng, C.-K. Multiscale entropy analysis of complex physiologic time series. *Phys. Rev. Lett.* **2002**, *89*, 068102. [CrossRef]
18. Ahmed, M.; Rehman, N.; Looney, D.; Rutkowski, T.; Mandic, D. Dynamical complexity of human responses: A multivariate data-adaptive framework. *Bull. Pol. Acad. Sci. Tech. Sci.* **2012**, *60*, 433–445. [CrossRef]
19. Costa, M.; Goldberger, A.L.; Peng, C.-K. Multiscale entropy analysis of biological signals. *Phys. Rev. E* **2005**, *71*, 021906. [CrossRef] [PubMed]
20. Silva, L.E.V.; Cabella, B.C.T.; da Costa Neves, U.P.; Junior, L.O.M. Multiscale entropy-based methods for heart rate variability complexity analysis. *Phys. A Stat. Mech. Its Appl.* **2015**, *422*, 143–152. [CrossRef]
21. Fogedby, H. On the phase space approach to complexity. *J. Stat. Phys.* **1992**, *69*, 411–425. [CrossRef]
22. Ahmed, M.U.; Mandic, D.P. Multivariate multiscale entropy analysis. *IEEE Signal Process. Lett.* **2012**, *19*, 91–94. [CrossRef]
23. Humeau-Heurtier, A. Multivariate refined composite multiscale entropy analysis. *Phys. Lett. A* **2016**, *380*, 1426–1431. [CrossRef]
24. Ahmed, M.U.; Mandic, D.P. Multivariate multiscale entropy: A tool for complexity analysis of multichannel data. *Phys. Rev. E* **2011**, *84*, 061918. [CrossRef] [PubMed]

25. Costa, M.D.; Goldberger, A.L. Generalized multiscale entropy analysis: Application to quantifying the complex volatility of human heartbeat time series. *Entropy* **2015**, *17*, 1197–1203. [CrossRef] [PubMed]
26. Stam, C.; Montez, T.; Jones, B.; Rombouts, S.; Van Der Made, Y.; Pijnenburg, Y.; Scheltens, P. Disturbed fluctuations of resting state EEG synchronization in Alzheimer's disease. *Clin. Neurophysiol.* **2005**, *116*, 708–715. [CrossRef] [PubMed]
27. Mizuno, T.; Takahashi, T.; Cho, R.Y.; Kikuchi, M.; Murata, T.; Takahashi, K.; Wada, Y. Assessment of EEG dynamical complexity in alzheimer's disease using multiscale entropy. *Clin. Neurophysiol.* **2010**, *121*, 1438–1446. [CrossRef]
28. Humeau-Heurtier, A. The multiscale entropy algorithm and its variants: A review. *Entropy* **2015**, *17*, 3110–3123. [CrossRef]
29. Takahashi, T.; Cho, R.Y.; Mizuno, T.; Kikuchi, M.; Murata, T.; Takahashi, K.; Wada, Y. Antipsychotics reverse abnormal EEG complexity in drug-naive schizophrenia: A multiscale entropy analysis. *Neuroimage* **2010**, *51*, 173–182. [CrossRef] [PubMed]
30. Ouyang, G.; Dang, C.; Li, X. Multiscale entropy analysis of EEG recordings in epileptic rats. *Biomed. Eng. Appl. Basis Commun.* **2009**, *21*, 169–176. [CrossRef]
31. Chung, C.-C.; Kang, J.-H.; Yuan, R.-Y.; Wu, D.; Chen, C.-C.; Chi, N.-F.; Chen, P.-C.; Hu, C.-J. Multiscale entropy analysis of electroencephalography during sleep in patients with parkinson disease. *Clin. EEG Neurosci.* **2013**. [CrossRef] [PubMed]
32. Azami, H.; Smith, K.; Fernandez, A.; Escudero, J. Evaluation of resting-state magnetoencephalogram complexity in Alzheimer's disease with multivariate multiscale permutation and sample entropies. In Proceedings of the 2015 37th Annual International Conference of the IEEE Engineering in Medicine and Biology Society (EMBC), Milan, Italy, 5–29 August 2015; pp. 7422–7425.
33. McKhann, G.; Drachman, D.; Folstein, M.; Katzman, R.; Price, D.; Stadlan, E.M. Clinical diagnosis of Alzheimer's disease: Report of the nincds-adrda work group* under the auspices of department of health and human services task force on Alzheimer's disease. *Neurology* **1984**, *34*, 939. [CrossRef] [PubMed]
34. Folstein, M.F.; Folstein, S.E.; McHugh, P.R. "Mini-mental state": A practical method for grading the cognitive state of patients for the clinician. *J. Psychiatr. Res.* **1975**, *12*, 189–198. [CrossRef]
35. Abásolo, D.; Escudero, J.; Hornero, R.; Gómez, C.; Espino, P. Approximate entropy and auto mutual information analysis of the electroencephalogram in alzheimer's disease patients. *Med. Biol. Eng. Comput.* **2008**, *46*, 1019–1028. [CrossRef] [PubMed]
36. Abásolo, D.; Hornero, R.; Espino, P.; Alvarez, D.; Poza, J. Entropy analysis of the EEG background activity in Alzheimer's disease patients. *Physiol. Meas.* **2006**, *27*, 241. [CrossRef] [PubMed]
37. Humeau-Heurtier, A. Multivariate generalized multiscale entropy analysis. *Entropy* **2016**, *18*, 411. [CrossRef]
38. Morabito, F.C.; Labate, D.; La Foresta, F.; Bramanti, A.; Morabito, G.; Palamara, I. Multivariate multi-scale permutation entropy for complexity analysis of alzheimer's disease EEG. *Entropy* **2012**, *14*, 1186–1202. [CrossRef]
39. Cao, L.; Mees, A.; Judd, K. Dynamics from multivariate time series. *Phys. D Nonlinear Phenom.* **1998**, *121*, 75–88. [CrossRef]
40. Pincus, S.M.; Goldberger, A.L. Physiological time-series analysis: What does regularity quantify? *Am. J. Physiol. Heart Circ. Physiol.* **1994**, *266*, H1643–H1656.
41. Azami, H.; Escudero, J. Refined composite multivariate generalized multiscale fuzzy entropy: A tool for complexity analysis of multichannel signals. *Phys. A Stat. Mech. Its Appl.* **2017**, *465*, 261–276. [CrossRef]
42. Valencia, J.F.; Porta, A.; Vallverdú, M.; Claria, F.; Baranowski, R.; Orlowska-Baranowska, E.; Caminal, P. Refined multiscale entropy: Application to 24-h holter recordings of heart period variability in healthy and aortic stenosis subjects. *IEEE Trans. Biomed. Eng.* **2009**, *56*, 2202–2213. [CrossRef] [PubMed]
43. Morabito, F.C.; Labate, D.; Bramanti, A.; La Foresta, F.; Morabito, G.; Palamara, I.; Szu, H.H. Enhanced compressibility of EEG signal in Alzheimer's disease patients. *IEEE Sens. J.* **2013**, *13*, 3255–3262. [CrossRef]
44. Yang, A.C.; Wang, S.-J.; Lai, K.-L.; Tsai, C.-F.; Yang, C.-H.; Hwang, J.-P.; Lo, M.-T.; Huang, N.E.; Peng, C.-K.; Fuh, J.-L. Cognitive and neuropsychiatric correlates of EEG dynamic complexity in patients with Alzheimer's disease. *Prog. Neuro Psychopharmacol. Biol. Psychiatry* **2013**, *47*, 52–61. [CrossRef] [PubMed]
45. Hornero, R.; Abásolo, D.; Escudero, J.; Gómez, C. Nonlinear analysis of electroencephalogram and magnetoencephalogram recordings in patients with Alzheimer's disease. *Philos. Trans. R. Soc. A Math. Phys. Eng. Sci.* **2009**, *367*, 317–336. [CrossRef] [PubMed]

46. Courtiol, J.; Perdikis, D.; Petkoski, S.; Müller, V.; Huys, R.; Sleimen-Malkoun, R.; Jirsa, V.K. The multiscale entropy: Guidelines for use and interpretation in brain signal analysis. *J. Neurosci. Methods* **2016**, *273*, 175–190. [CrossRef] [PubMed]
47. Rish, I. An empirical study of the naive bayes classifier. In *IJCAI 2001 Workshop on Empirical Methods in Artificial Intelligence*; IBM: New York, NY, USA, 2001; pp. 41–46.
48. Hall, M.; Frank, E.; Holmes, G.; Pfahringer, B.; Reutemann, P.; Witten, I.H. The weka data mining software: An update. *ACM SIGKDD Explor. Newslett.* **2009**, *11*, 10–18. [CrossRef]
49. Jelles, B.; Van Birgelen, J.; Slaets, J.; Hekster, R.; Jonkman, E.; Stam, C. Decrease of non-linear structure in the EEG of alzheimer patients compared to healthy controls. *Clin. Neurophysiol.* **1999**, *110*, 1159–1167. [CrossRef]
50. Kyriazis, M. Practical applications of chaos theory to the modulation of human ageing: Nature prefers chaos to regularity. *Biogerontology* **2003**, *4*, 75–90. [CrossRef] [PubMed]
51. Abásolo, D.; Hornero, R.; Gómez, C.; García, M.; López, M. Analysis of EEG background activity in Alzheimer's disease patients with lempel–ziv complexity and central tendency measure. *Med. Eng. Phys.* **2006**, *28*, 315–322. [CrossRef] [PubMed]